Journal of Applied Electrochemistry **33**: 675–684, 2003.

A mathematical model of multiple ion transport across an ion-selective membrane under current load conditions

V. FÍLA and K. BOUZEK*
*Department of Inorganic Technology, Institute of Chemical Technology, Technická 5, 16628 Prague 6, Czech Republic (*author for correspondence, e-mail: karel.bouzek@vscht.cz)*

Received 12 September 2002; accepted in revised form 27 February 2003

Key words: current load, diffusion, ion-selective membrane, ion transport, mathematical model

Abstract

A macrohomogeneous mathematical model of the simultaneous transport of multiple ions across an ion exchange membrane based on the Nernst–Planck equation was developed. Schlögl's equation of motion was used to evaluate the convective term of the mass-transfer inside the membrane. The model accounts for the external diffusion of the ions through the Nernst diffusion layer to the phase boundary on both sides of the membrane. Donnan equilibrium is used to describe the potential and the concentration discontinuity on the membrane-solution interface. The results document the importance of the external diffusion layers for ion transport across the membrane.

List of symbols

c molar concentration (mol m^{-3})
d_e equivalent diameter (m)
F Faraday number (C mol^{-1})
j current density (A m^{-2})
k membrane permeability (m^2)
$\bar{k}$ mass transfer coefficient (m s^{-1})
L membrane length (m)
N molar flux (mol m^{-2} s^{-1})
p pressure (Pa)
R universal gas constant (J K^{-1} mol^{-1})
T temperature (K)
$\mathbf{v}$ fluid flow velocity (m s^{-1})
x coordinate (m)
z charge number (-)

Dimensionless criterions

Re Reynolds number, $Re = vd_e\rho/\eta$
Sc Schmidt number, $Sc = \eta/D\rho$
Sh Sherwood number, $Sh = \bar{k}d_e/D$

Greek letters

δ thickness of Nernst diffusion or membrane layer (m)
η electrolyte dynamic viscosity (kg m^{-1} s^{-1})
φ Galvani potential (V)
ϕ source (mol m^{-3} s^{-1})
ρ density (kg m^{-3})
τ time (s)

Subscripts

a anolyte
c catholyte
l liquid phase
M membrane
s solid phase

1. Introduction

Ion-selective membranes have found a wide range of applications in electrochemical technologies, such as chlor-alkali electrolysis, electrodialysis [1] and more recently low temperature fuel cells [2]. Even though they are widely used in practice, the principle of their function and mass-transfer behaviour has not yet been completely understood.

Numerous studies have been published dealing with the structure of perfluorinated sulfonated membranes [3–11]. The aim was to understand membrane internal structure in order to explain their transport properties. In the last decade mathematical models have often been used to verify various mechanisms of mass transfer across the membranes. The emphasis has been mainly on proton exchange membrane (PEM) fuel cells [12–18]. A study of the electric potential distribution inside a Nafion® membrane during water electrolysis has also been made [19].

The majority deal with perfluorinated ionomeric membranes applied in chlor-alkali electrolysis. The major advantages of this process when compared to the two competitive technologies (mercury and diaphragm electrolysis) are the lower energy consumption, high purity of caustic produced and lower environmental impact. Therefore 90% of all planned chlor-alkali industry expansion is in ion-exchange membrane cell

processes [20,21]. Several reviews describing this technology in more detail have been published [22]. Correspondingly, a series of studies have been published addressing the critical aspects of this process. The most important contributions are summarized in [23]. One critical aspect identified is the purity of the brine fed into the anode compartment. Contamination of the brine by the alkaline earth cations from crude salt results in the rapid deterioration of the membrane properties [24]. Concentrations higher than 1×10^{-7} g dm^{-3} are sufficient to seriously damage the expensive membrane. Several studies have been published concerning the properties of membranes in the environment of the chlor-alkali electrolysis process in an attempt to explain the behaviour of the membrane [25, 26].

Similarly to fuel cell research, in this case, too, mathematical modeling has proven to be an efficient tool for optimization of the electrolysis process. Three basic types of mathematical model have been reported [23] based on: (i) the macrohomogeneous model, (ii) irreversible thermodynamics and (iii) absolute reaction rates.

The macrohomogeneous model is characterized by parameters that can be obtained directly from experiments. Their results are directly applicable to industrial problems. The disadvantage is that this model averages all parameters in the total membrane volume, which is generally larger than the dimension of the pores. The application of the macrohomogeneous model for simulation of mass transfer across the membranes has been the subject of numerous studies [23, 27–29].

The irreversible thermodynamic approach is characterized by the transport parameters, which can only be obtained experimentally with difficulty. The models based on this theory therefore generally allow for the fact that the parameters have to be estimated. Although this approach permits a description of the mass transfer inside the membrane, at present it does not generally provide quantitative results. The most widely used method using this approach is based on the Stefan–Maxwell equations [30, 31].

Models based on the theory of absolute reaction rates have not been used widely because of the extremely complicated mathematics and the lack of a direct connection to industrial problems [32].

Several studies evaluating ion transport through the membrane consider it to consist of cylindrical pores with an electrical charge fixed on the walls [33–37]. They represent a separate group.

The papers published so far in the field of mass transfer across the membrane in the chlor-alkali electrolysis cell only account for the membrane. The fixed known concentration of individual ions at the membrane surface (from the side of the membrane interior) is considered. However, as has been shown by Kelsall et al. [38], concentrations of individual ions exhibit great changes across the Nernst diffusion layer at the membrane surface. This also applies to the pH of the solution. Variation of this parameter may result in the undesirable decomposition of the hypochlorite produced in an industrial cell to chlorate ions. It is obvious that the local concentration changes near the membrane surface will significantly influence the mass transfer behaviour of the membrane. The aim of this paper is to verify this theory and to contribute to a deeper understanding of the processes taking place in an industrial chlor-alkali electrochemical reactor.

2. Mathematical model description

In the present work a macrohomogeneous model was employed. The direct impact of this approach to industrial problems and its validity have been verified, for example, by Verbrugge and Hill [39]. The ion transport was evaluated using the Nernst–Planck equation,

$$\mathbf{N}_i = -D_i \nabla c_i - c_i \left(\frac{D_i}{RT}\right) z_i F \nabla \varphi + c_i \mathbf{v} \tag{1}$$

where the ion mobility was eliminated by means of the Nernst–Einstein equation,

$$u_i = \frac{z_i F D_i}{RT} \tag{2}$$

The material balance for an ion can be written as

$$\frac{\partial c_i}{\partial \tau} = \phi_i - \operatorname{div} N_i \tag{3}$$

By integrating Equation 1 into Equation 3, the material balance equation takes the form

$$\frac{\partial c_i}{\partial \tau} = \phi_i - \operatorname{div}\left(-D_i \nabla c_i - c_i \left(\frac{D_i}{RT}\right) z_i F \nabla \varphi + c_i \mathbf{v}\right) \tag{4}$$

Considering the stationary state and the absence of chemical reactions, Equation 4 simplifies to

$$0 = \operatorname{div}\left(-D_i \nabla c_i - c_i \left(\frac{D_i}{RT}\right) z_i F \nabla \varphi + c_i \mathbf{v}\right) \tag{5}$$

The pore flow velocity $\mathbf{v}$ of the electrolyte solution can be expressed using the modified Schlögl equation [12].

$$\mathbf{v} = \frac{k}{\eta_{\mathrm{M}}} (z_{\mathrm{M}} c_{\mathrm{M}} F \nabla \varphi - \nabla p) \tag{6}$$

By introducing Equation 6 into Equation 5, the final relationship for the ion i balance in the membrane can be expressed as

$$0 = \operatorname{div}\left(-D_i \nabla c_i - c_i \left(\frac{D_i}{RT}\right) z_i F \nabla \varphi + c_i \frac{k}{\eta_{\mathrm{M}}} (z_{\mathrm{M}} c_{\mathrm{M}} F \nabla \varphi - \nabla p)\right) \tag{7}$$

In the Nernst diffusion layer outside the membrane, the convective mass transfer term was neglected during the calculations and the balance equation leads to

$$0 = \mathrm{div}\left(-D_i \nabla c_i - c_i \left(\frac{D_i}{RT}\right) z_i F \nabla \varphi\right) \tag{8}$$

From the point of view of the mass conservation law the convective flux should be considered in the Nernst diffusion layer. We attempted to consider this during the calculations but were not successful due to the divergence of the numerical mathematical methods used. Convective flux was therefore omitted in the external diffusion layer.

The electrical current density load can be expressed as

$$j = F \sum_{i}^{N_{ions}} z_i N_i \tag{9}$$

The electroneutrality condition is given by Equation 10 for the membrane interior and by Equation 11 for the diffusion film:

$$\sum_{i}^{N_{ions}} z_i c_i + z_{\mathrm{M}} c_{\mathrm{M}} = 0 \tag{10}$$

$$\sum_{i}^{N_{ions}} z_i c_i = 0 \tag{11}$$

In the mathematical model comprising both the membrane interior and the outer electrolyte boundary layer, the evaluation of the concentrations and the potential discontinuity at the interfaces is difficult. In the present work, the expression for the Donnan potential was used to overcome this problem,

$$\Delta\varphi_{Don}^{(\mathrm{s},\mathrm{l}_k)} = \varphi^{(\mathrm{s})} - \varphi^{(\mathrm{l}_k)} = \frac{RT}{F} \ln\left[\frac{c_i^{(\mathrm{l}_k)}}{c_i^{(\mathrm{s})}}\right]^{1/z_i} \quad k = 1, 2 \tag{12}$$

For the location of individual interfaces see Figure 1. The activity coefficients of the individual ions were considered to be unity in the whole system under study. Equation 12 provides a relationship between the concentrations of any ion on the respective sides of the membrane-free electrolyte interface.

Assuming incompressibility of the liquid phase, that is,

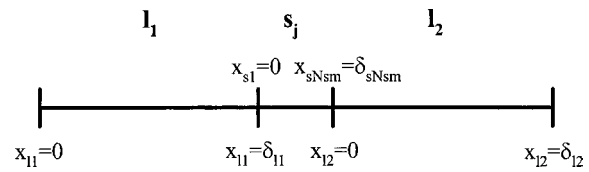

Fig. 1. Schematic sketch of the system. Symbol **l** indicates electrolyte boundary layers, **s** the membrane layer.

$$\mathrm{div}\, v = 0 \tag{13}$$

Equation 6 can be used to obtain the relationship for the pressure profile inside the membrane

$$0 = \frac{k}{\eta_{\mathrm{M}}} \left(z_{\mathrm{M}} c_{\mathrm{M}} F \nabla^2 \varphi - \nabla^2 p\right) \tag{14}$$

This equation is valid, assuming c_{M} and z_{M} are independent of the position.

The following boundary conditions were used (cf. Figure 1 for the symbols):

$$\mathbf{c}^{(\mathrm{l}_1)}\big|_{x_{\mathrm{l}_1}=0} = \mathbf{c}^{(1)} \tag{15}$$

$$\mathbf{c}^{(\mathrm{l}_2)}\big|_{x_{\mathrm{l}_2}=\delta_{\mathrm{l}_2}} = \mathbf{c}^{(2)} \tag{16}$$

$$\varphi^{(\mathrm{l}_1)}\big|_{x_{\mathrm{l}_1}=0} = 0 \tag{17}$$

$$p^{(\mathrm{s})}\big|_{x_{\mathrm{s}}=0} = p^{(1)} \tag{18}$$

$$p^{(\mathrm{s})}\big|_{x_{\mathrm{s}}=\delta_{\mathrm{s}}} = p^{(2)} \tag{19}$$

At the solution–membrane interface the following set of boundary conditions was used:

$$\Delta\varphi_{Don}^{(\mathrm{s},\mathrm{l}_1)} = \varphi^{(\mathrm{s})}\big|_{x_{\mathrm{s}}=0} - \varphi^{(\mathrm{l}_1)}\big|_{x_{\mathrm{l}_1}=\delta_{\mathrm{l}_1}} = \frac{RT}{F} \ln\left[\frac{c_i^{(\mathrm{l}_1)}\big|_{x_{\mathrm{l}_1}=\delta_{\mathrm{l}_1}}}{c_i^{(\mathrm{s})}\big|_{x_{\mathrm{s}}=0}}\right]^{1/z_i} \tag{20}$$

$$\sum_{i}^{N_{ions}} z_i c_i^{(\mathrm{s})}\big|_{x_{\mathrm{s}}=0} + z_{\mathrm{M}} c_{\mathrm{M}} = 0 \tag{21}$$

$$\mathbf{N}_i\big|_{x_{\mathrm{l}_1}=\delta_{\mathrm{l}_1}} = \mathbf{N}_i\big|_{x_{\mathrm{s}}=0} \tag{22}$$

On the membrane–solution interface the conditions take the following form:

$$\Delta\varphi_{Don}^{(\mathrm{l}_2,\mathrm{s})} = \varphi^{(\mathrm{l}_2)}\big|_{x_{\mathrm{l}_2}=0} - \varphi^{(\mathrm{s})}\big|_{x_{\mathrm{s}}=\delta_{\mathrm{s}}} = \frac{RT}{F} \ln\left[\frac{c_i^{(\mathrm{s})}\big|_{x_{\mathrm{s}}=\delta_{\mathrm{s}}}}{c_i^{(\mathrm{l}_2)}\big|_{x_{\mathrm{l}_2}=0}}\right]^{1/z_i} \tag{23}$$

$$\sum_{i}^{N_{ions}} z_i c_i^{(\mathrm{l}_2)}\big|_{x_{\mathrm{l}_2}=0} = 0 \tag{24}$$

$$\mathbf{N}_i\big|_{x_{\mathrm{l}_2}=0} = \mathbf{N}_i\big|_{x_{\mathrm{s}}=\delta_{\mathrm{s}}} \tag{25}$$

Assuming that the electrolyte flow is laminar, the average thickness of the Nernst diffusion layer can be

calculated using an expression proposed by Roušar et al. [40].

$$Sh = 1.85\left(\frac{d_e}{L} \times Re \times Sc\right)^{1/3} \quad (26)$$

The above set of algebraic-differential equations (DAEs) was solved by a shooting method. In the individual sections, the set of equations was integrated using the multistep implicit method based on the BDF Gears formulae suitable for difficult problems (library procedure DDASPK [41]). During integration of DAEs using DDASPK a numerical difficulty was encountered when the inconsistent initial values of independent variables were used. An initialisation procedure was developed to handle this issue.

The distribution of the concentrations on the electrolyte–membrane interfaces was evaluated using the ZREAL [42] library procedure designed to calculate the roots of real function. The set of non-linear equations resulting from the principle of the shooting method was solved by using the Newton–Raphson method.

2.1. *Input parameters*

In the present model the behaviour of the perfluorinated sulfonated membrane Nafion® 117 was simulated. This membrane was chosen in spite of the fact it is not used in modern chlor-alkali electrolytic cells because of its low selectivity when compared with bilayer perfluoro-sulphonic/carboxylic membranes. The reason was the availability of the input parameters. Nafion® 117 is a membrane that has been studied for many years with various parameters published in the literature. This is not the case with modern bilayer membranes. Nevertheless, assuming that reliable input parameters are available, the model presented is also able to cope with bilayer membranes.

The membrane thickness of 1.2×10^{-4} m, permeability $k = 1.58 \times 10^{-19}$ m^2 [12], concentration of fixed functional groups $c_M = 1.2 \times 10^3$ mol m^{-3} and their valence $z_M = -1$ were used in the present work. For the NaCl solution the viscosity value of 1.87×10^{-3} kg m^{-1} s^{-1} given in [43] was used, for NaOH solution viscosity in cathode compartment a value of 2.79×10^{-2} kg m^{-1} s^{-1}, and for the pore fluid viscosity an average value of the catholyte and anolyte of 1.48×10^{-2} kg m^{-1} s^{-1}. The following values of the Reynolds number were considered inside the electrode compartments: $Re_a = 0.11$ and $Re_c = 7.5 \times 10^{-3}$. These values were calculated for the arbitrarily set electrolyte flow rate in the anode and cathode compartments of 1.7×10^{-2} m s^{-1}. The value of the Reynolds number valid for the industrial cell is difficult to obtain. The mass transfer coefficient in this system has been the subject of numerous studies [44].

The values of the diffusion coefficients in the membrane and solutions under conditions close to industrial brine electrolysis pose further problems. The majority of studies on diffusion coefficients focus on diluted solutions where the Donnan exclusion is fulfilled and the concentration conditions inside the membrane are well defined. The lack of information relevant to industrial conditions was noted by Yeager et al. [45, 46] who estimated the self-diffusion coefficient of sodium [45] and chloride [46] ions in the Nafion® membrane under conditions close to those of industrial electrolysis. Diffusion coefficients were estimated in the concentrated sodium chloride and hydroxide solution. In the present work the values for the 9.5 M NaOH solution $D_{Na^+,M} = 3.52 \times 10^{-11}$ m^2 s^{-1} and 10 M NaOH solution $D_{Cl^-,M} = 1.29 \times 10^{-11}$ m^2 s^{-1} at 80 °C were applied. The diffusion coefficients for the membrane immersed in the NaOH solution were used. This was because during experiments in which the membrane separates the NaCl and NaOH solutions it was found that the properties of the side of the membrane in contact with the NaOH solution dominate the overall membrane performance [45]. The proton self-diffusion coefficient is difficult to determine even under mild laboratory conditions. This is because marked hydrogen isotopes may also diffuse through the membrane in the form of water molecules. In the present study the proton diffusion coefficient dependence on the number of water molecules per ion exchange site in the membrane published by Zawodzinski et al. [47] was used. The number of water molecules was evaluated from the water content in the membrane in dependence on the concentration of the external NaOH solution given in [45]. For the conditions simulated during this study it has a value of approximately 6. This swelling of the membranes corresponds to $D_{H^+,M} = 3.7 \times 10^{-10}$ m^2 s^{-1}. For the hydroxyl ion diffusion a coefficient value of $D_{OH^-,M} = 5.20 \times 10^{-11}$ m^2 s^{-1} obtained by Narebska et al. [48] was chosen for the 4 M NaOH as the external electrolyte at 60 °C. The values of the diffusion coefficient were obtained from the membrane conductivity data using irreversible thermodynamics of transport across a charged membrane. No data on the transport of Ca^{2+} across the Nafion® membrane under industrial conditions were found. Therefore, the value of $D_{Ca^{2+},M} = 7.09 \times 10^{-11}$ m^2 s^{-1} published by Xue et al. [49] was used in the present work. It was obtained using a rotating diffusion cell, 0.2 M HCl solution on one side of the membrane and various $CaCl_2$ concentrations on the opposite one. The Ca^{2+} flux densities were extrapolated to the high cell rotation rate and high $CaCl_2$ concentration.

Diffusion coefficient values of various ions in the anolyte solution were studied in order to evaluate the chlorine chemistry in the hydrodynamic layer near the membrane. In the present study the following data published by Kelsall et al. [38] were used: $D_{Cl^-,a} = 2.03 \times 10^{-9}$ m^2 s^{-1}, $D_{H^+,a} = 9.31 \times 10^{-9}$ m^2 s^{-1} and $D_{OH^-,a} = 5.26 \times 10^{-9}$ m^2 s^{-1}. No data were found for the remaining ions. Therefore the following data valid for the diluted water solution were selected: $D_{Na^+,a} = 1.33 \times 10^{-9}$ m^2 s^{-1} and $D_{Ca^{2+},a} = 7.92 \times 10^{-10}$ m s^{-1}.

For the catholyte the following values published by Easteal and Woolf [50] for 19 M NaOH at 40 °C were used: $D_{H^+,c} = 1.47 \times 10^{-10}$ m^2 s^{-1} and $D_{OH^-,c} = 2.72 \times 10^{-10}$ m^2 s^{-1}. The remaining data were once again not found. The values were selected with regard to the qualitative similarity of the anolyte and catholyte properties. The ratio of the values of D_{OH^-} coefficients in the catholyte and anolyte was calculated. The values of diffusion coefficients in the catholyte were obtained by multiplying those in the anolyte by the ratio. The following values were obtained: $D_{Cl^-,c} = 1.08 \times 10^{-10}$ m^2 s^{-1}, $D_{OH^-,c} = 2.72 \times 10^{-10}$ m^2 s^{-1} and $D_{Ca^{2+},c} = 4.10 \times 10^{-11}$ m^2 s^{-1}.

3. Results and discussion

Using the mathematical model the behaviour of the systems close to the brine electrolysis process was simulated. The pH of the 5 M brine solution on the anode side was set equal to 2 and to contain 0.2 mM $CaCl_2$. The catholyte was 13 M NaOH. The model parameters were varied so as to obtain information on the behaviour of the model and membrane performance under different conditions.

The calculated concentration profiles at increasing current load for the three ions with the highest concentration, that is, Na^+, OH^- and Cl^-, are shown in Figures 2 to 4, respectively. The corresponding molar flux densities are summarized in Figure 5. Under open circuit conditions Na^+ and OH^- concentration gradients are the main driving force of the mass transfer across the membrane. This is in agreement with the calculated Na^+ concentration profile across the system under zero current load. The apparent concentration decrease in the direction from the cathode to the anode is quite evident (see Figure 2). Consequently, the qualitatively identical concentration profile was also calculated for the OH^- ion. This is shown in Figure 3. With increasing current load the effect of electric field intensity becomes important and Na^+ flux gradually turns in the opposite direction. At a current load of about 400 A m^{-2} the migration and convective transport of Na^+ prevail over diffusion. However, as follows from Figure 5, the increased portion of the electrical charge is transported by OH^- ion. Its molar flux density is enhanced by the increasing strength of the electric field and exceeds that

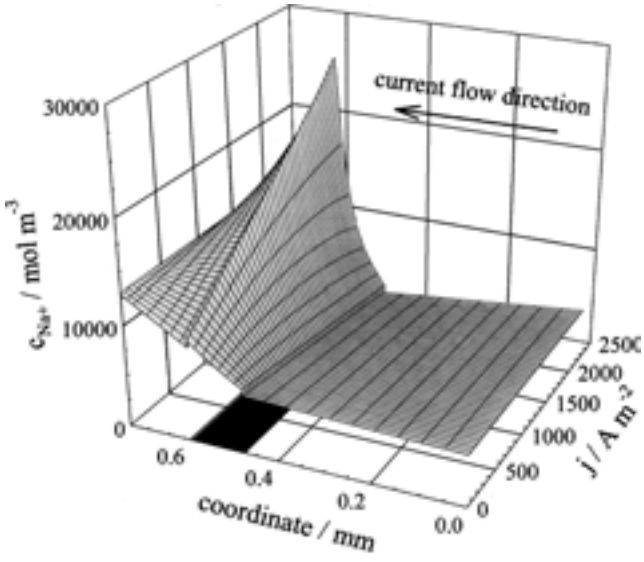

Fig. 2. Concentration profiles of the Na^+ ion at various current densities; anolyte: 5000 mol NaCl m^{-3}, 0.2 mol $CaCl_2$ m^{-3}, pH 2; catholyte: 13 000 mol NaOH m^{-3}. Black field at bottom indicates membrane region. Current flows in direction of coordinate *x*.

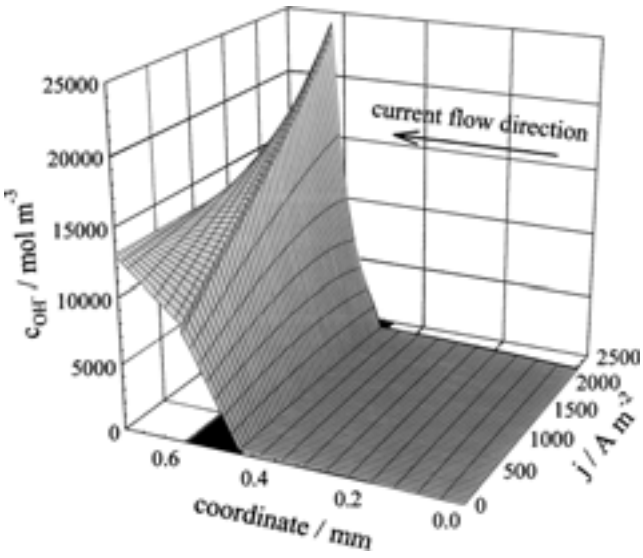

Fig. 3. Concentration profiles of the OH^- ion at various current densities; anolyte: 5000 mol NaCl m^{-3}, 0.2 mol $CaCl_2$ m^{-3}, pH 2; catholyte: 13 000 mol NaOH m^{-3}. Black field at bottom indicates membrane region. Current flows in direction of coordinate *x*.

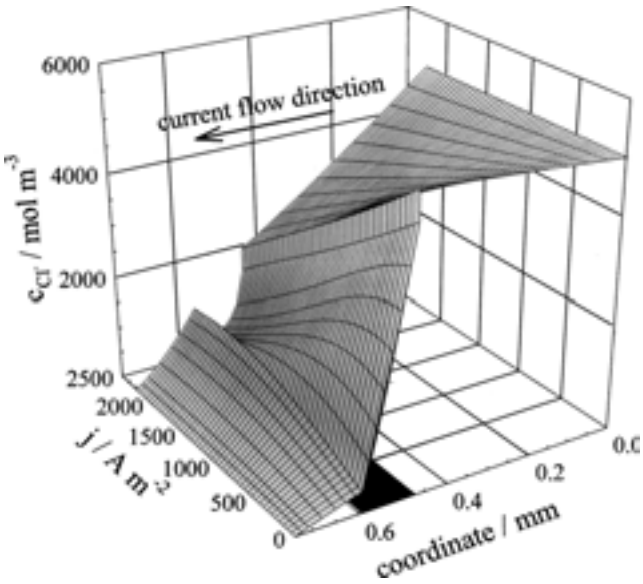

Fig. 4. Concentration profiles of the Cl^- ion at various current densities; anolyte: 5000 mol NaCl m^{-3}, 0.2 mol $CaCl_2$ m^{-3}, pH 2; catholyte: 13 000 mol NaOH m^{-3}. Black field at bottom indicates membrane region. Current flows in direction of coordinate *x*.

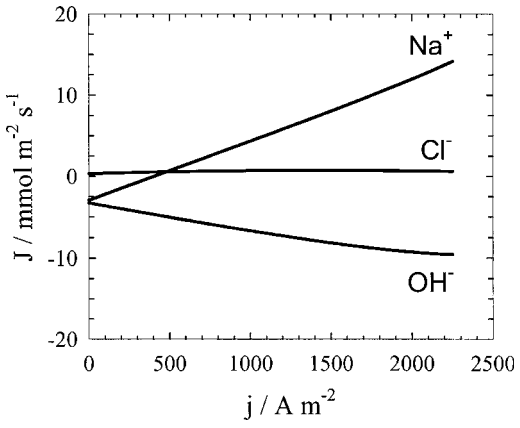

Fig. 5. Molar flux densities of Na^+, OH^- and Cl^- ions at various current densities; anolyte: 5000 mol NaCl m^{-3}, 0.2 mol $CaCl_2$ m^{-3}, pH 2; catholyte: 13 000 mol NaOH m^{-3}. Flow in direction of coordinate x (Figures 2 to 4) is considered positive.

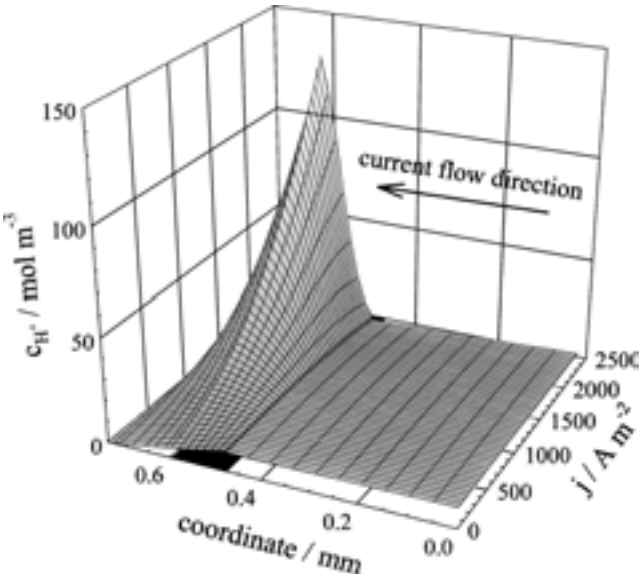

Fig. 6. Concentration profiles of the H^+ ion at various current densities; anolyte: 5000 mol NaCl m^{-3}, 0.2 mol $CaCl_2$ m^{-3}, pH 2; catholyte: 13 000 mol NaOH m^{-3}. Black field at bottom indicates membrane region. Current flows in direction of coordinate x.

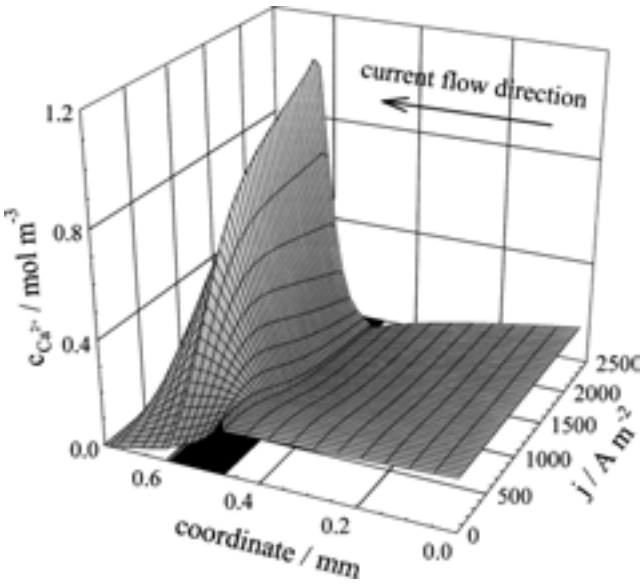

Fig. 7. Concentration profiles of the Ca^{2+} ion at various current densities; anolyte: 5000 mol NaCl m^{-3}, 0.2 mol $CaCl_2$ m^{-3}, pH 2; catholyte: 13 000 mol NaOH m^{-3}. Black field at bottom indicates membrane region. Current flows in direction of coordinate x.

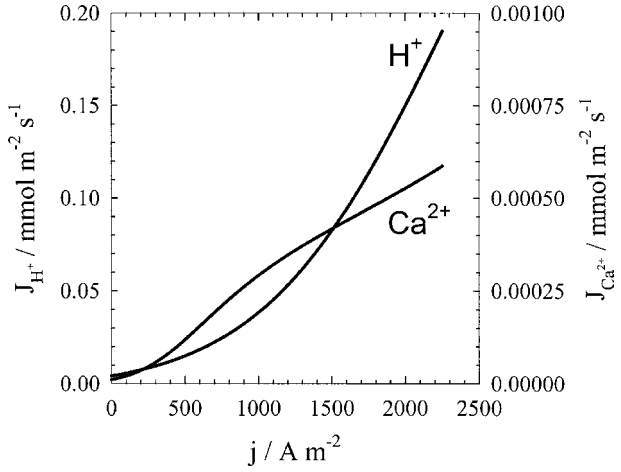

Fig. 8. Molar flux densities of H^+ and Ca^{2+} ions at various current densities; anolyte: 5000 mol NaCl m^{-3}, 0.2 mol $CaCl_2$ m^{-3}, pH 2; catholyte: 13 000 mol NaOH m^{-3}. Flow in direction of coordinate x (Figures 6 and 7) is considered positive.

of the Na^+ ion up to a current load of 1550 A m^{-2}. The concentration profiles of both ions change significantly. The Na^+ concentration profile follows changes in its flux density as shown in Figure 2. OH^- concentration in the catholyte behaves similarly in order to maintain electroneutrality. On the anode side the situation is more complex. The other species which plays an important role in the electroneutrality of the solution is the Cl^- ion. In spite of the decreasing flux density of this ion, with increasing current load its concentration profile in the anolyte changes markedly across the diffusion layer; this is connected with the electroneutrality problem.

The remaining ions (H^+ and Ca^{2+}) do not play an important part in the charge transfer process and do not directly influence the selectivity of the membrane. The concentration profiles of these ions inside the membrane as well as in the electrolyte are vital for the assessment of membrane stability under particular conditions. They allow an assessment of the tendency of the membrane to adversely affect its transport properties. Calculated concentration profiles and molar flux densities are shown in Figures 6–8. Important changes in the concentration profiles inside the Nernst diffusion film take place at higher current densities, where the intensity of ion transport across the membrane starts to increase. These changes are generally more pronounced in the catholyte. Two interesting features follow from the concentration profiles. The first is the course of the surface concentrations of both ions in the anode compartment with increasing current load. Proton concentration increases with increasing current load

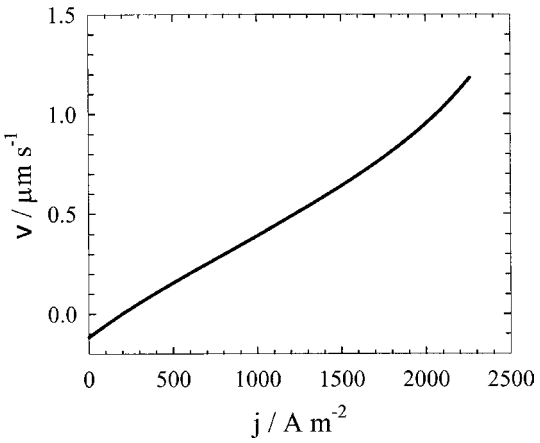

Fig. 9. Pore fluid flow rate at various current densities; anolyte: 5000 mol NaCl m^{-3}, 0.2 mol $CaCl_2$ m^{-3}, pH 2; catholyte: 13 000 mol NaOH m^{-3}. Flow in direction of coordinate x is considered positive.

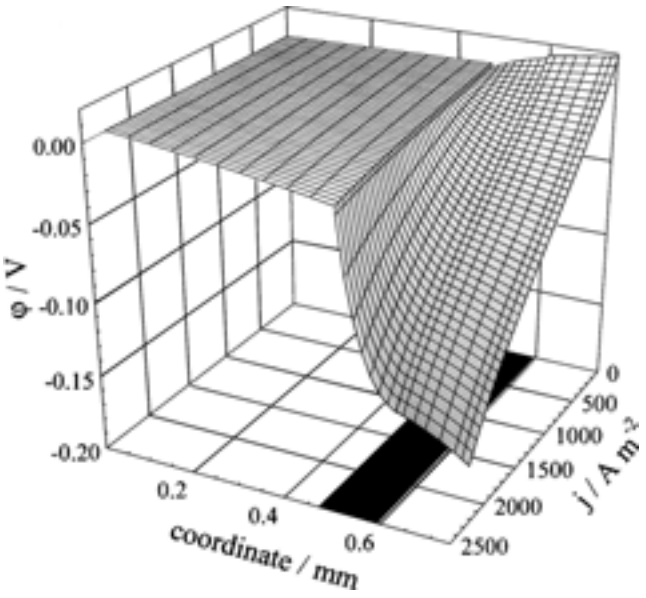

Fig. 10. Galvani potential profiles at various current densities; anolyte: 5000 mol NaCl m^{-3}, 0.2 mol $CaCl_2$ m^{-3}, pH 2; catholyte: 13 000 mol NaOH m^{-3}. Black field at bottom indicates membrane region. Current flows in direction of coordinate x.

and flux density across the membrane, that is, the trend is the very opposite of that expected. In this case, too, the reason is the necessity to fulfil the electroneutrality condition. With enhanced current loads the concentration of Ca^{2+} reaches a maximum at the interface between the membrane and the catholyte. The significant increase in Ca^{2+} concentration in the interior of the membrane is an important factor with regard to its sorption on the fixed functional groups. This may lead to a serious local deterioration of the properties of the membrane. Ca^{2+} precipitation in the form of hydroxide is an additional danger. As follows from a comparison of Figures 3 and 6, this model does not maintain the water dissociation equilibrium constant. The water dissociation constant was not considered because of serious numerical complications encountered after the addition of a further algebraic equation to the model. Moreover, it does not provide any evident advantage in terms of accuracy of results because the ion activity coefficient is set to unity. This is a complex problem which cannot be handled separately. Further study, including the water dissociation constant and the activity coefficients of individual ions inside the membrane, is necessary in order to quantify processes connected with Ca^{2+} diffusion into the membrane, its sorption and possibly also its precipitation.

The velocity of the electroosmotic flow through the membrane vs. current load is shown in Figure 9. Under zero current conditions the electroosmotic flux is negative due to the liquid junction potential. With increasing current load it increases and reaches a zero value at approximately 200 A m^{-2}. This is connected with the increasing electric field strength inside the membrane, as shown in Figure 10. In spite of the increasing electroosmotic flow, OH^- transport remains an important factor. At a current density of 2250 A m^{-2} approximately 60%

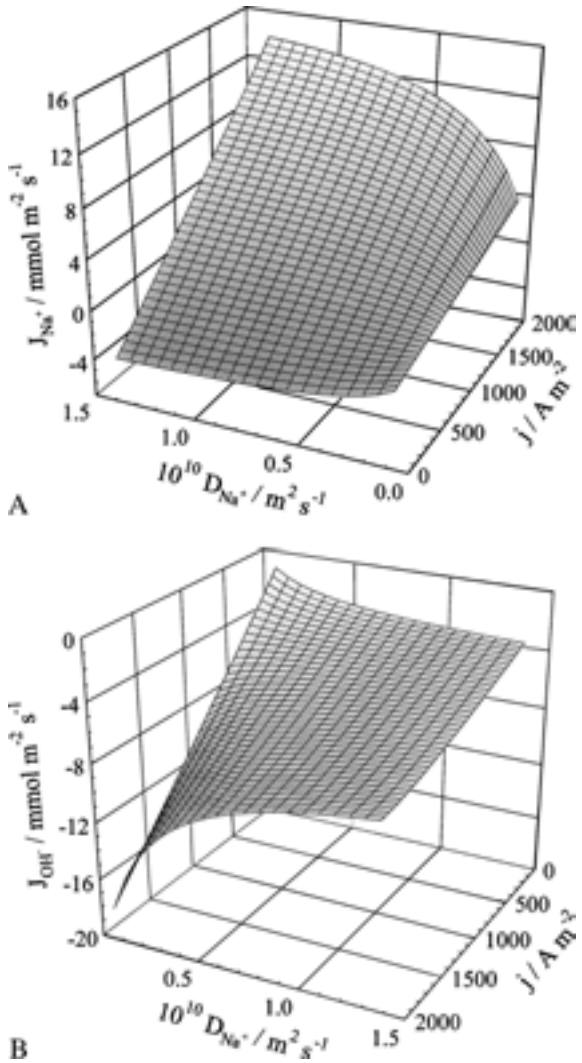

Fig. 11. Molar flux densities of (A) Na^+ and (B) OH^- at various current densities and $D_{Na^+,c}$; anolyte: 5000 mol NaCl m^{-3}, 0.2 mol $CaCl_2$ m^{-3}, pH 2; catholyte: 13 000 mol NaOH m^{-3}. Flow in direction of coordinate x is considered positive.

of the electrical charge flowing through the cell corresponds to the transport of the Na^+ ion from the anolyte into the catholyte. A current efficiency of approximately 40% was found experimentally [51]. There are several possible reasons for this discrepancy. The first is the values of the diffusion coefficients. As mentioned in the chapter on input parameters, several values of the diffusion coefficients were not found in the literature for the conditions relevant to this study. The most important was $D_{Na^+,c}$ in the catholyte solution. This may introduce a crucial error into the set of input data used. A parametric study of the Na^+ diffusion coefficient value in the catholyte was performed. The results are summarized in Figure 11A,B. As shown, the reduction of the $D_{Na^+,c}$ value causes exponential decay in membrane selectivity. At a current load of 1600 A m^{-2} and $D_{Na^+,c} = 6.88 \times 10^{-12}$ m^2 s^{-1} only 15% of the electrical charge flowing was used for the Na^+ transport from the anolyte into the catholyte. For $D_{Na^+,c}=1.38\times10^{-10}$ m^2 s^{-1} this increased to 61%. A similar dependence of ionic flux may be observed for the variation of the D_{OH^-} value. For $D_{OH^-,c}=2.72\times10^{-10}$ m^2 s^{-1} the flux of Na^+ ion corresponded to 53% of the current load of 1600 A m^{-2}. If the $D_{OH^-,c}$ value is reduced to 2.72×10^{-11} m^2 s^{-1} the Na^+ flux represents 74% of the current load and inversely for $D_{OH^-,c}$ of 5.44×10^{-10} m^2 s^{-1} 48%. With increasing $D_{Na^+,c}$ value the influence of the electric field on OH^- flux density is severely reduced.

The other important parameter is the ratio k/η_m representing the physically inverse value of membrane hydraulic resistivity. A membrane permeability k value was published by Verbrugge and Hill [12]. Pore fluid viscosity is difficult to determine experimentally. An average value based on the catholyte and anolyte solution was used in the present study. In reality the influence of Donnan exclusion on the electrolyte composition inside the membrane pores has to be taken into account. This may change the value of this parameter significantly. Moreover, it may be position dependent. A parametric study of the ratio k/η_M was performed. The results are summarised in Figure 12A–C. As shown in Figure 12A, the enhanced value of the ratio results in a more extended variation of the pore fluid flow velocity with the current load. An important feature is the exponential increase in fluid flow at high ratio and current load values. The dependence of Na^+ flux density on current load remains approximately linear for the ratio values studied. Only at the highest values was a slight enhancement at high current loads observed. This compensates for the deterioration of the OH^- transport, which is well visible in Figure 12C, for the identical parameter range. This is connected with the exponential increase in electroosmotic electrolyte flow at high current densities and high ratio values. This phenomenon results in the enhanced selectivity of the membrane. At a current density of 1600 A m^{-2} and k/η_M ratio of 1.52×10^{-17} kg m^3 s^{-1} 73% of the current load is used to transport Na^+ from the anolyte to the catholyte.

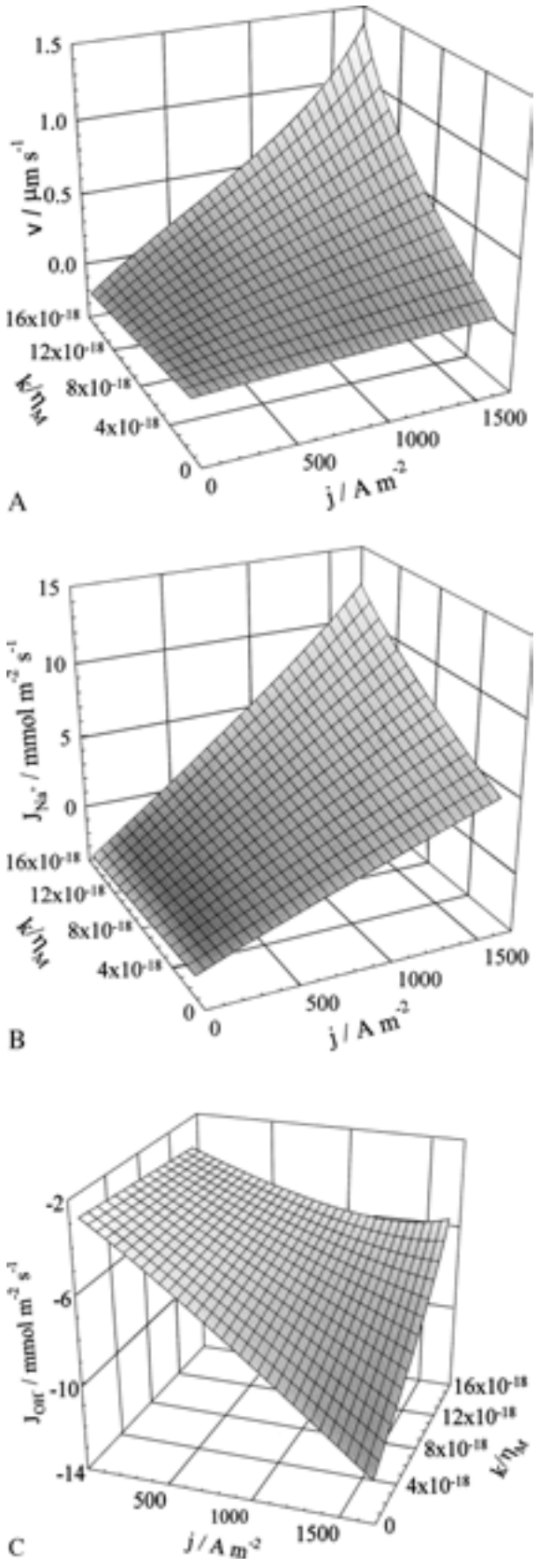

Fig. 12. (A) Pore fluid flow rate and molar flux densities of (B) Na^+ and (C) OH^- at various current densities and k/η_M ratio; anolyte: 5000 mol NaCl m^{-3}, 0.2 mol $CaCl_2$ m^{-3}, pH 2; catholyte: 13 000 mol NaOH m^{-3}. Flow in direction of coordinate x is considered positive.

The results obtained clearly indicate lower membrane selectivity compared with industrial applications. There are several reasons for this: (a) bilayer membranes with enhanced selectivity are used in the brine electrolysis industry; (b) selectivity is strongly influenced by the input parameters and current density used, as shown in Figures 11 and 12; further study is needed to set their values correctly; (c) activity coefficients can in fact differ from unity, this parameter is supposed to play an important role in the superselectivity of perfluorinated sulphonated membranes [26]; (d) due to the stability of the numerical method the current densities used in industrial cells were not attained in the present case. Increasing current density enhances membrane selectivity.

4. Conclusions

The mathematical model shows the importance of the external diffusion layers on ion transfer across the ion exchange membrane. The discrepancy between the model and experimental data was explained by the deviation of the input parameters from the real conditions and the neglect of ion activity coefficients in the membrane, as well as in the free solution.

The model provides interesting information on the Ca^{2+} distribution inside the membrane. This is of special importance to those dealing with membrane deterioration. In order to quantify the results water dissociation in the membrane has to be taken into account. This problem is complicated by the fact that the kinetics of water dissociation may also play an important part.

Acknowledgements

The financial support of this research by the Grant Agency of the Czech Republic under project number 203/99/0575 and by the Ministry of Education, Youth and Sports under project number CEZ: MSM223100001 is gratefully acknowledged.

References

1. D. Pletcher and F. Walsh, 'Industrial Electrochemistry' (Chapman & Hall, London 1990).
2. K. Kordesch and G. Simander, 'Fuel Cells and Their Applications' (VCH, Weinheim 1996).
3. F. Helfferich, 'Ion Exchange' (McGraw-Hill, New York, 1962).
4. H.L. Yeager and A. Steck, *J. Electrochem. Soc.* **128** (1981) 1880.
5. H.L. Yeager, Z. Twardowski and L.M. Clarke, *J. Electrochem. Soc.* **129** (1982) 324.
6. A. Eisenberg and H.L. Yeager (Eds), 'Perfluorinated Ionomer Membranes', ACS Symp. Ser. 180 (American Chemical Society, Washington DC, 1982).
7. R.S. Yeo, *J. Electrochem. Soc.* **130** (1983) 533.
8. M. Mulder, 'Basic Principles of Membrane Technology' (Kluwer Academic, Dordrecht, The Netherlands, 1991).
9. S. Schlick (Ed.), 'Ionomers Characterization Theory and Applications' (CRC Press, New York, 1996).
10. J. Divisek, M. Eikerling, V. Mazin, H. Schmitz, U. Stimming and Yu.M. Volfkovich, *J. Electrochem. Soc.* **145** (1998) 2677.
11. H.-G. Haubold, Th. Vad, H. Jungbluth and P. Hiller, *Electrochim. Acta* **46** (2001) 1559.
12. M.W. Verbrugge and R.F. Hill, *J. Electrochem. Soc.* **137** (1990) 886.
13. M.W. Verbrugge and R.F. Hill, *J. Electrochem. Soc.* **137** (1990) 893.
14. M.W. Verbrugge and R.F. Hill, *J. Electrochem. Soc.* **137** (1990) 1131.
15. M. Eikerling, Yu.I. Kharkats, A.A. Kornyshev and Yu.M. Volfkovich, *J. Electrochem. Soc.* **145** (1998) 2684.
16. S.J. Paddison, R. Paul and T.A. Zawodzinski Jr, *J. Electrochem. Soc.* **147** (2000) 617.
17. T. Thampan, S. Malhotra, H. Tang and R. Datta, *J. Electrochem. Soc.* **147** (2000) 3242.
18. S. Um, C-Y. Wang and K.S. Chen, *J. Electrochem. Soc.* **147** (2000) 4485.
19. P. Millet, *Electrochim. Acta* **39** (1994) 2501.
20. l.C. Curlin, T.V. Bommaraju and C.B. Hansson, 'Kirk–Othmer Encyclopedia of Chemical Technology' Vol. 1 (J. Wiley & Sons, New York, 1991) p. 938.
21. C-P. Chen and B.V. Tilak, *J. Appl. Electrochem.* **26** (1996) 235.
22. M. Seko, A. Yomiyama and A. Ogawa, *in* R.E. White (Ed.), 'Electrochemical Cell Design' (Plenum, New York, 1984), p. 135.
23. G. Pillay, 'Mathematical Modelling of Macrohomogeneous Transport Phenomena in Ion-Exchange Membranes', PhD thesis, (New Mexico State University, 1993).
24. Y. Ogata, T. Kojima, S. Uchiyama, M. Yasuda and H. Fine, *J. Electrochem. Soc.* **136** (1989) 91.
25. K. Kimoto, *J. Electrochem. Soc.* **130** (1983) 334.
26. R.R. Chandran, R.S. Yeo and D-T. Chin, *Electrochim. Acta* **30** (1985) 1585.
27. R. Schlögl, *Ber. Bunsenges. Phys. Chem.* **70** (1966) 400.
28. T.R. Brumleve and R.P. Buck, *J. Electroanal. Chem.* **90** (1978) 1.
29. M.W. Verbrugge and P.N. Pintauro, *in*: B.E. Conway, J.O'M. Bockris and R.E. White (Eds), 'Modern Aspects of Electrochemistry', Vol. 19 (Plenum, New York, 1989), pp. 1–67.
30. P.N. Pintauro, PhD thesis (University of California, Los Angeles, CA, 1980).
31. J.A. Hogendoorn, A.J. van der Veen, J.H.G. van der Stegen, J.A.M. Kuipers and G.F. Versteeg, *Comput. Chem. Eng.* **25** (2001) 1251.
32. N. Lakshminarayanaiah, 'Transport Phenomena in Membranes' (Academic, New York, 1969).
33. V. Sasidhar and E. Ruckenstein, *J. Coll. Interface Sci.* **85** (1982) 332.
34. E.H. Cwirko and R.G. Carbonell, *J. Coll. Interface Sci.* **129** (1989) 513.
35. E.H. Cwirko and R.G. Carbonell, *J. Membr. Sci.* **48** (1990) 155.
36. E.H. Cwirko and R.G. Carbonell, *J. Membr. Sci.* **67** (1992) 211.
37. E.H. Cwirko and R.G. Carbonell, *J. Membr. Sci.* **67** (1992) 227.
38. R.T. Leah, N.P. Brandon, V. Vesovic and G.H. Kelsall, *J. Electrochem. Soc.* **147** (2000) 4173.
39. M.W. Verbrugge and R.F. Hill, *Electrochim. Acta* **37** (1992) 221.
40. I. Roušar, J. Hostomský, V. Cezner and B. Štverák, *J. Electrochem. Soc.* **118** (1971) 881.
41. P.N. Brown, A.C. Hindmarsh and L.R. Petzold, 'Consistent Initial Condition Calculation for Differential-Algebraic Systems' LLNL Report UCRL-JC-122175 (Aug. 1995).
42. IMSL Numerical Library (1994).
43. D.R. Lide (Ed.), 'CRC Handbook of Chemistry and Physics', 78th edn (CRC, New York, 1997).
44. M.J. Schmidt, A.A. Wragg, L.J. Janssen and K. Bouzek, Mass transfer and reaction distribution in a gas evolving narrow-gap electrolysis cell with lantern blade electrodes, 2nd European Congress of Chemical Engineering, Montpellier, France (Oct. 1999).
45. H.L. Yeager, B. Kipling and R.L. Dotson, *J. Electrochem. Soc.* **127** (1980) 303.

46. A. Herrera and H.L. Yeager, *J. Electrochem. Soc.* **134** (1987) 2446.
47. T.A. Zawodzinski, M. Neeman, L.O. Sillerud and S. Gottesfeld, *J. Phys. Chem.* **95** (1991) 6040.
48. A. Narebska, W. Kujawski and S. Koter, *J. Membr. Sci.* **30** (1987) 125.
49. T. Xue, R.B. Longwell and K. Osseo-Asare, *J. Membr. Sci.* **58** (1991) 175.
50. A.J. Easteal and L.A. Woolf, *J. Phys. Chem.* **90** (1986) 2441.
51. R. Bork-Brücken and K.H. Simmrock, *Chem. Ing. Tech.* **58** (1986) 407.